Daily Electrical Silencing in the Mammalian Circadian Clock

Mino D. C. Belle, *et al.*

Science **326**, 281 (2009);
DOI: 10.1126/science.1169657

tremes, eutriconodonts, and the living therians, and this ancestral feature is retained in eutriconodonts and spalacotheroids; but DMME evolved in extant monotremes (*14*) and in multituberculates for a second time, and then again for a third time in marsupials and placentals.

Paedomorphosis, or retention of fetal or juvenile characteristics of ancestors and/or relatives through developmental heterochrony, is a common phenomenon in vertebrate evolution. Scenario i gains support from the paedomorphic similarity of the ossified Meckel's cartilage in eutriconodonts and spalacotheroids to that of extant mammalian embryos (*15*). The premature ossification of Meckel's cartilage represents a simple developmental change in timing (heterochrony), for which a genetic mechanism has been established (*29*, *30*).

A mutant genetic and signaling network that can result in a premature ossification of Meckel's cartilage in mammalian embryogenesis has been characterized by recent genetic studies. Meckel's cartilage derives from cranial neural crest cells; it serves as scaffolding for development of mandibular and middle ear elements. Normal development of the Meckel's cartilage and its derivatives in vertebrates requires a wide range of structural and homeobox genes, such as *Bapx1*, *Gsc*, *Emx2*, *Sox9*, and *Type II Col.*, which are expressed in the mammalian middle ear structure [reviewed by (*30*)]. Morphogenesis of Meckel's cartilage also requires a variety of growth factors, some of which are ubiquitous in mammalian development. This complex signaling network for Meckel's normal development includes transforming growth factors–β (*Tgf*-β) (*29*), connective tissue growth factors (*Ctgf*) (*29*), fibroblast growth factor (*Fgf*) (*30*), epidermal growth factor (*Egf*) (*31*), and bone morphogenetic proteins (*Bmp*), among others.

In normal chondrogenesis of Meckel's cartilage of *Mus* (wild type), the signaling pathway from *Tgf*-β (upstream) to *Ctgf* (downstream) stimulates the proliferation, and inhibits the terminal differentiation, of chondrocytes (*29*). Mutant *Tgfbr2* $^{fl/fl}$*;Wnt1-Cre* genes (a mutant of *Tgf*-β) accelerate chondrocyte proliferation and cause ossification of Meckel's cartilage in mutant *Mus* (*29*). The phenotype of ossified Meckel's cartilage in *Tgfbr2* $^{fl/fl}$*;Wnt1-Cre* mutant mice is similar to the fossilized and (prematurely) ossified Meckel's cartilage in the spalacotheroids (Fig. 2) and eutriconodonts (Fig. 3). This suggests that some similar developmental pathway had underlined the ossification of Meckel's cartilage in extinct Mesozoic mammals.

Among living mammals, an ossified Meckel's cartilage occurs only in certain mutant mice; the cartilage is retained only in pathological cases among humans. However, ossified Meckel's cartilage evolved at least twice in Mesozoic spalacotheroids and eutriconodonts. The absence of ossified Meckel's cartilage in the adult in extant monotremes, marsupials, and placentals represents a more-canalized development of the middle ear for these living lineages, in contrast to a much more labile evolutionary development of middle ear features, made possible by a greater diversity of about 20 Mesozoic mammaliaform clades (*1*, *5*).

References and Notes

1. Z. Kielan-Jaworowska, R. L. Cifelli, Z.-X. Luo, *Mammals from the Age of Dinosaurs—Origins, Evolution, and Structure* (Columbia Univ. Press, New York, 2004).
2. Z.-X. Luo *et al.*, *Acta Palaeontol. Pol.* **47**, 1 (2002).
3. T. Martin, O. W. M. Rauhut, *J. Vertebr. Paleontol.* **25**, 414 (2005).
4. G. W. Rougier *et al.*, *American Mus. Nov.* **3566**, 1 (2007).
5. Z.-X. Luo, *Nature* **450**, 1011 (2007).
6. C. L. Cifelli, S. K. Madsen, *Geodiversitas* **21**, 167 (1999).
7. T. Tsubamoto *et al.*, *Acta Palaeontol. Pol.* **49**, 329 (2004).
8. S. C. Sweetman, *Palaeontology* **51**, 1367 (2008).
9. G. W. Rougier *et al.*, *Acta Geol. Sin.* **77**, 7 (2003).
10. G. Li, Z.-X. Luo, *Nature* **439**, 195 (2006).
11. E. F. Allin, J. A. Hopson, "The auditory apparatus of advanced mammal-like reptiles and early mammals," in *The Evolutionary Biology of Hearing*, D. B. Webster, *et al.*, Eds. (Springer-Verlag, New York, 1992), pp. 587–614.
12. J. Meng *et al.*, *Zool. J. Linn. Soc.* **138**, 431 (2003).
13. C.-K. Li *et al.*, *Chinese Sci. Bull. (English Ed.)* **48,** 1129 (2003).
14. T. H. Rich, J. A. Hopson, A. M. Musser, T. F. Flannery, P. Vickers-Rich, *Science* **307**, 910 (2005).
15. Z.-X. Luo *et al.*, *Nature* **446**, 288 (2007).
16. T. Rowe *et al.*, *Proc. Natl. Acad. Sci. U.S.A.* **105**, 1238 (2008).
17. Systematics: Class Mammalia; Clade Trechnotheria (*1*); Superfamily Spalacotheroidea (*9*, *10*); Family *Zhangheotheriidae*; Genus *Maotherium* (*10*); sp. nov. *Maotherium asiaticus*. Holotype: Henan Geological Museum, Zhengzhou, China (HGM 41H-III-0321; Figs. 1 and 2), an almost complete skull, and most of the postcranial skeleton. Etymology: *asiaticus*, Latin for the Asiatic provenance of zhangheotheriids. Locality and Age: Lujiatun Locality (120°54′41″E, 41°36′26″N), Beipiao, Liaoning Province, China; the Yixian Formation. The site dated to be 123.2 ± 1.0 million years old (*22*). Diagnosis: I3, C1, P1, M5; i3, c1, p1, m6. *M. asiaticus* is referred to *Maotherium* by apomorphies shared by *Maotherium sinensis* (type species): deep precondylar notch of mandible, a deep ectoflexus on upper molars with cusp B′, a gradient in increasingly acute angle in triangulation of molar cusps toward the posterior molar, sigmoidal shape of the posterior ventral border of mandible. Differs from *M. sinensis* in having apomorphies of low central cusp between B′ and C; *M. asiaticus* has the tibial distal styloid process and the proximolateral process of the metatarsal 5 (all three features absent in *M. sinensis*). Full diagnosis in (*22*).
18. Z.-X. Luo, A. W. Crompton, A.-L. Sun, *Science* **292**, 1535 (2001).
19. Z.-X. Luo, J. R. Wible, *Science* **308**, 103 (2005).
20. Q. Ji, Z.-X. Luo, C.-X. Yuan, A. R. Tabrum, *Science* **311**, 1123 (2006).
21. J. Meng *et al.*, *Nature* **444**, 889 (2006).
22. Materials and methods are available as supporting material on *Science* Online.
23. E. C. Kirk *et al.*, *J. Hum. Evol.* **55**, 278 (2008).
24. Z.-X. Luo, Q. Ji, J. R. Wible, C.-X. Yuan, *Science* **302**, 1934 (2003).
25. W. Maier, in *Mammal Phylogeny*, F. S. Szalay *et al.*, Eds. (Springer-Verlag, New York, 1993), vol. 1, pp. 165–181.
26. M. R. Sánchez-Villagra *et al.*, *J. Morphol.* **251**, 219 (2002).
27. T. Rowe, *Science* **273**, 651 (1996).
28. J. Meng, A. R. Wyss, *Nature* **377**, 141 (1995).
29. K. Oka *et al.*, *Dev. Biol.* **303**, 391 (2007).
30. A. S. Tucker *et al.*, *Development* **131**, 1235 (2004).
31. L. Shum *et al.*, *Development* **118**, 903 (1999).

32. We thank G. Cui for fossil preparation; M. R. Dawson for improving the manuscript; and R. Asher, Y. Chai, and A. Tucker for discussion. Support from the 973 Project of Ministry of Science and Technology of China (Q.J.); from Institute of Geology of Chinese Academy of Geological Sciences (Beijing) (C.-X.Y.), from NSF (USA), National Natural Science Foundation (China), and National Geographic Society (Z.-X.L.); and from Henan Provincial Government (to Z.-L.Z. and L.X.).

Supporting Online Material

www.sciencemag.org/cgi/content/full/326/5950/278/DC1
Materials and Methods
SOM Text
References

1 July 2009; accepted 17 August 2009
10.1126/science.1178501

Daily Electrical Silencing in the Mammalian Circadian Clock

Mino D. C. Belle,[1] Casey O. Diekman,[2,4] Daniel B. Forger,[3,4] Hugh D. Piggins[1]*

Neurons in the brain's suprachiasmatic nuclei (SCNs), which control the timing of daily rhythms, are thought to encode time of day by changing their firing frequency, with high rates during the day and lower rates at night. Some SCN neurons express a key clock gene, *period 1* (*per1*). We found that during the day, neurons containing *per1* sustain an electrically excited state and do not fire, whereas non-*per1* neurons show the previously reported daily variation in firing activity. Using a combined experimental and theoretical approach, we explain how ionic currents lead to the unusual electrophysiological behaviors of *per1* cells, which unlike other mammalian brain cells can survive and function at depolarized states.

In mammals, behavior and physiology are regulated on a daily basis by the brain's master circadian (~24-hour) clock in the suprachiasmatic nuclei (SCNs). The *period 1* (*per1*) gene is a key component of the molecular mechanism of this clock (*1*); its expression in the SCN peaks during the day and is low at night, and can be used as a marker of clock-containing SCN neurons and their circadian phase (*2*, *3*). SCN neurons are also thought to express time of day by changing their firing frequency, with high rates during the day and lower rates at night (*4*–*6*). A fundamental question in circadian biology is how the intracellular molecular circadian clock regulates the electrophysiology of SCN neurons. A Hodgkin-Huxley–type model of SCN neurons shows that circadian changes in ionic conductances can account for the circadian variation

in firing rate (*7*). This model also predicts that the molecular clock can drive SCN neurons to exhibit an unusual depolarized rest state not previously reported experimentally. Because not all SCN neurons appear to contain the molecular clock machinery (*8*), a further prediction of this model is that SCN neurons that express the key clock genes (such as *per1*) will have different electrical properties than those that do not express these genes.

To measure time-dependent changes in the membrane properties and excitability of SCN neurons in vitro, and to investigate potential differences among these neurons, we made targeted whole-cell recordings from SCN of mice expressing an enhanced green fluorescent protein (EGFP) reporter of *per1*. We sampled from 309 "*per1*" neurons showing detectable EGFP and 109 neurons in which EGFP could not be detected ("non-*per1*"). We found a marked difference in the electrophysiological behavior during the day of these two populations.

Sampling from *per1* and non-*per1* neurons throughout the SCN across the projected day-night cycle revealed large circadian variation in resting membrane potential (RMP), membrane input resistance (R_{input}), and overall electrophysiological behaviors (Figs. 1 and 2). In the morning [Zeitgeber Time (ZT) 2 to 4.25, where ZT0 represents lights-on and ZT12 represents lights-off], *per1* neurons were at moderate RMP (V_m = –44 ± 0.6 mV; n = 47 neurons) and generated action potentials (APs) (4.3 ± 0.1 Hz) (Figs. 1 and 2). In the afternoon (ZT5.25 to 10.75), *per1* neurons were spontaneously depolarized and either showed low-amplitude 2- to 7-Hz oscillations in membrane potential (MP) (mean V_m = –35 ± 0.7 mV; n = 50 neurons) or were completely silent (V_m = –27 ± 0.4 mV; n = 50 neurons) (Figs. 1 and 2). Around dusk (ZT10.75 to 12.75), these cells were again at moderate RMP (–46 ± 1 mV; n = 45 neurons) and generated APs, but at lower frequency than in the morning (1 ± 0.1 Hz) (Figs. 1 and 2). This progression from moderate RMP in the morning to depolarized states (–25 to –34 mV) in the afternoon and back to moderate RMP at dusk was specific to *per1* neurons; non-*per1* cells remained at moderate RMP (V_m = –46 ± 0.9 mV; n = 48 neurons) and continued to generate APs until dusk (Figs. 1 and 2). In contrast, during the early night (ZT13 to 15.25) both *per1* and non-*per1* neurons became robustly hyperpolarized and showed no APs (*per1*, –68 ± 0.5 mV; n = 40 neurons; non-*per1*, –66 ± 1.1 mV; n = 24 neurons), but later in the night (ZT16.75 to 23) both *per1* and non-*per1* neurons were at or close to moderate RMP and generated APs (Figs. 1 and 2).

In many studies, unusually depolarized neurons are considered unhealthy, so we were careful to establish that such *per1* neurons were physiologically sound. Indeed, depolarized states were only observed in cells recorded during the afternoon and never in cells tested in morning, dusk, or night. Further, silent *per1* cells characteristic of the state attained in the afternoon had extremely high R_{input} and, by application of steady-state hyperpolarizing currents, could be induced to fire regular APs like those of cells measured in the morning (R_{input} at –25 mV = 2.9 ± 0.1 gigohm, n = 38 neurons) (fig. S1). Alternatively, steady-state depolarizing currents reversibly silenced regular AP-firing *per1* cells in the morning, rendering them indistinguishable from neurons measured in the afternoon portion of the light cycle (n = 26 neurons) (fig. S1). Depolarization of non-*per1* neurons in a similar manner compromises their electrophysiological properties. Thus, *per1* neurons appear to be healthy and functioning within normal whole-cell electrophysiological parameters.

We used mathematical modeling to determine whether these observed electrical behaviors could be explained by existing data on the ionic currents measured within SCN neurons. To simulate *per1* neurons at various circadian phases, we first adapted a model of unidentified SCN neurons (*7*) to account for the enhanced electrical excitability of *per1* neurons (fig. S2). We then incorporated into the model circadian variations in K^+ and Ca^{2+} conductances (fig. S3), and intracellular Ca^{2+} concentration (fig. S4), from published experimental observations (*9*–*11*). Although a circadian variation in only one ionic current could cause transitions from a hyperpolarized

[1]Faculty of Life Sciences, A. V. Hill Building, University of Manchester, Manchester M13 9PT, UK. [2]Department of Industrial and Operations Engineering, University of Michigan, Ann Arbor, MI 48109, USA. [3]Department of Mathematics, University of Michigan, Ann Arbor, MI 48109, USA. [4]Center for Computational Medicine and Bioinformatics, University of Michigan, Ann Arbor, MI 48109, USA.

*To whom correspondence should be addressed. E-mail: hugh.d.piggins@manchester.ac.uk

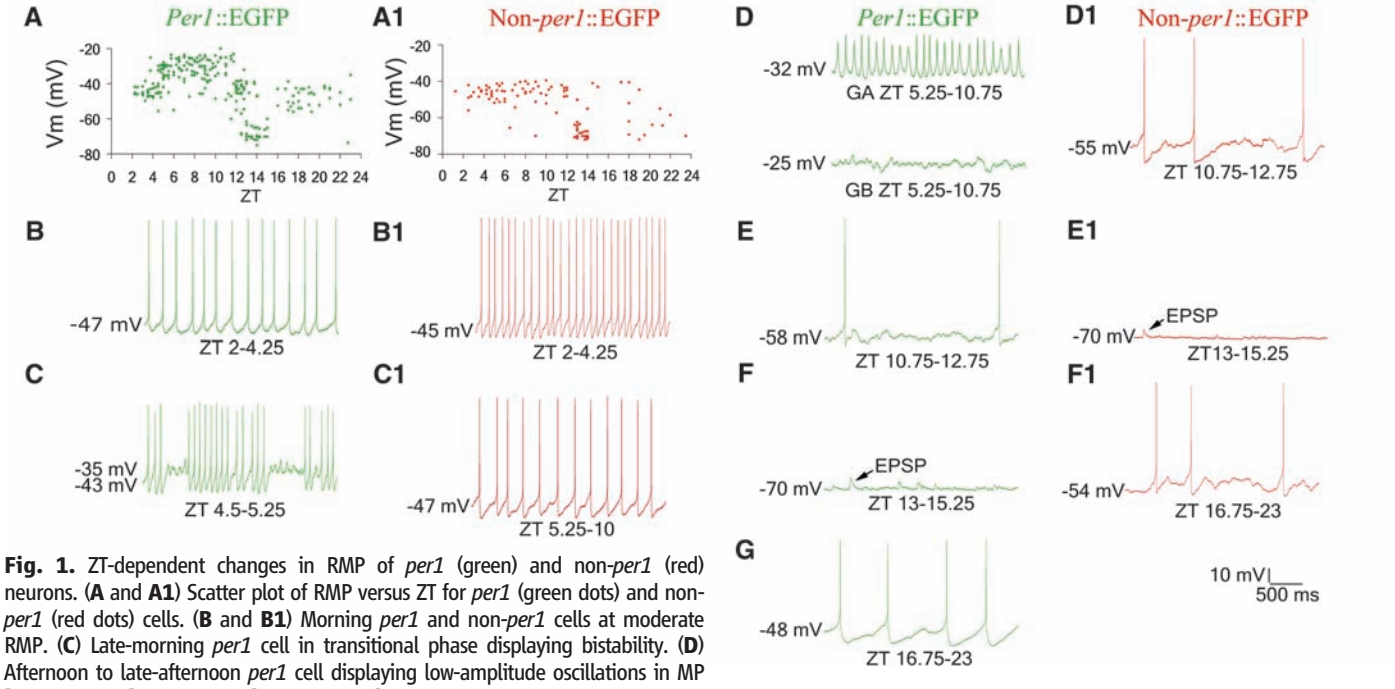

Fig. 1. ZT-dependent changes in RMP of *per1* (green) and non-*per1* (red) neurons. (**A** and **A1**) Scatter plot of RMP versus ZT for *per1* (green dots) and non-*per1* (red dots) cells. (**B** and **B1**) Morning *per1* and non-*per1* cells at moderate RMP. (**C**) Late-morning *per1* cell in transitional phase displaying bistability. (**D**) Afternoon to late-afternoon *per1* cell displaying low-amplitude oscillations in MP [group A (GA)] or silenced [group B (GB)] as determined by their R_{input} and electrophysiological behaviors (Fig. 2). (**C1**) Non-*per1* neurons do not display bistability or depolarized RMP, but remained at moderate RMP, generating APs. (**E** and **D1**) Dusk *per1* and non-*per1* cells at moderate RMP around the time of lights-off. (**F** and **E1**) Early night *per1* and non-*per1* cells hyperpolarized and silenced, receiving excitatory postsynaptic potentials (EPSPs). (**G** and **F1**) Late-night *per1* and non-*per1* neurons at moderate RMP.

steady state to repetitive firing, and also from repetitive firing to a depolarized steady state (figs. S5 and S6), circadian rhythms in both K^+ and Ca^{2+} currents were required to faithfully reproduce the fine details of these transitions (Fig. 1, B to G, and Fig. 3).

Mathematical analysis revealed that as the day progresses, transitions in the behavior of *per1* neurons occur when a quiescent state gains or loses stability through Hopf bifurcations (fig. S3). This common mathematical structure has been found in many other neural systems and corresponds to Type II excitability (spiking emerging with nonzero frequency) in Hodgkin's original classification system (*12*). The changes in stability of the hyperpolarized rest state we observed at night in *per1* neurons are similar in character to those seen in other neurons (*13*). However, *per1* neurons are different in that a second Hopf bifurcation occurs during the day, when an unusually depolarized rest state becomes stable or unstable. The physiological importance of these bifurcations is that minor, molecular clock–driven changes in certain ionic conductances can have a major effect on the bioelectrical output of the neuron. Near bifurcation points, neurons can exhibit the types of behaviors seen in *per1* neurons, such as low-amplitude oscillations in MP or noise-induced transitions between oscillatory and quiescent states (*12*, *14*). These behaviors do not appear to depend on the initial state of the neuron (fig. S3) and can be achieved with a variety of parameter choices (figs. S4, S5, S6, and S7).

In both *per1* and non-*per1* cells, the cyclical changes in RMP were closely associated and in phase with alterations in R_{input} (Fig. 2). For *per1* cells, the amplitude of the circadian variation in RMP and R_{input} were 42 mV [day, –27 ± 0.4 mV; night, –68 ± 0.5 mV; $P < 1 \times 10^{-5}$; all P values were determined by means of analysis of variance (ANOVA) and post-hoc Bonferroni test unless otherwise stated] and 2.1 gigohm (day, 2.9 ± 0.1 gigohm; night, 0.8 ± 0.03 gigohm; $P < 1 \times 10^{-5}$), respectively. The measured membrane time constant was also significantly larger during the day than at night (afternoon, 48.3 ms; early night, 23.3 ms; $P < 0.001$; $n = 20$ neurons). These differences between day and night *per1* cells were not associated with any change in cell capacitance (day, 9.4 ± 0.04 pF; night, 9.3 ± 0.05 pF; $n = 10$ neurons), and thus are not a result of changes in cell size. In non-*per1* cells, the differences in RMP and R_{input} between the day and night were 20 mV (day, –46 ± 0.9 mV; night, –66 ± 1.1 mV; $P < 0.001$) and 0.9 gigohm (day, 1.6 ± 0.1 gigohm; night, 0.7 ± 0.1 gigohm; $P < 0.001$), respectively.

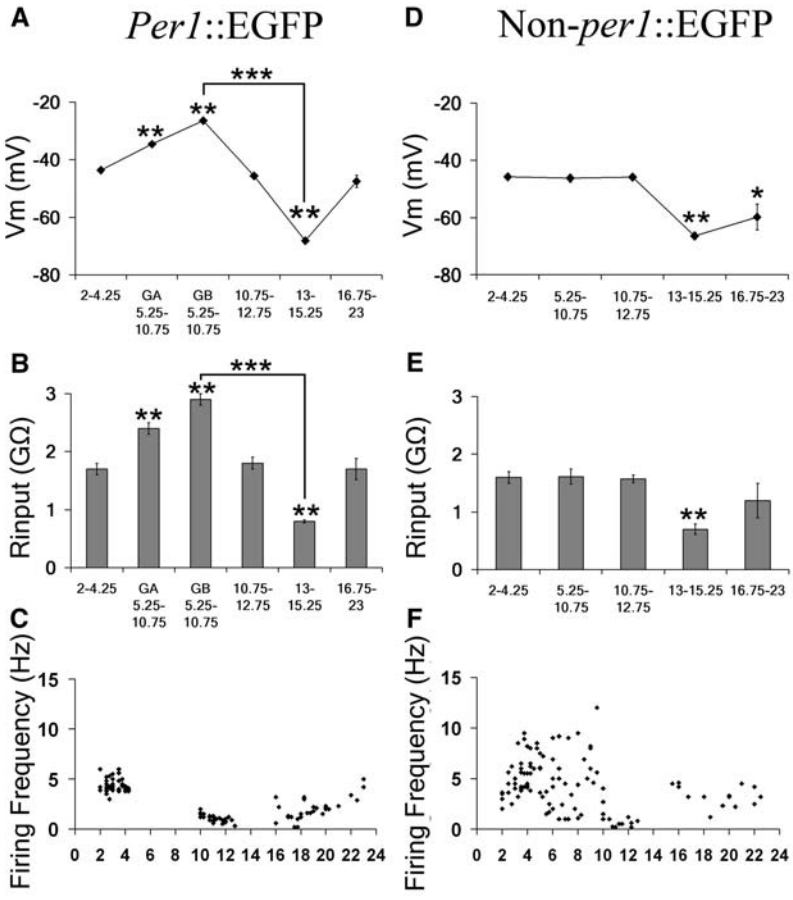

Fig. 2. Changes in RMP and associated changes in R_{input} and firing frequency of *per1* and non-*per1* cells across a day-night cycle. *Per1* cells in GA and GB at ZT5.25 to 10.75 were determined by their electrophysiological behaviors (Fig. 1) and R_{input} ($P < 0.01$) (Fig. 2B). GA cells displayed low-amplitude 2- to 7-Hz oscillations in MP, whereas GB cells were silent. (**A**) Changes in RMP of *per1* cells and (**B**) associated changes in their R_{input}. (**C**) Scatter plot of firing frequency versus ZT for *per1* cells, showing *per1* cells generating APs in the morning, at dusk, and during late night; however, *per1* cells were completely silent during the afternoon and early night. (**D**) Changes in RMP of non-*per1* cells, and (**E**) associated changes in their R_{input}. (**F**) Scatter plots of firing frequency versus ZT for non-*per1* cells, showing the previously reported daily variation in firing frequency of these cells. *$P < 0.05$; **$P < 0.001$; ***$P < 1 \times 10^{-5}$. Numerical data represent ±SEM

Our measurements and modeling indicate that a clock-controlled reduction in K^+ channel conductance causes depolarization in *per1* cells in the afternoon, and an increase in K^+ channel conductance at night causes the hyperpolarization. We also reasoned that L-type Ca^{2+} channels may contribute to determining the RMP of these cells (*9*, *15*, *16*). We therefore bath-applied tetraethylammonium (TEA; a broad spectrum K^+ channel blocker) or nimodipine (an L-type Ca^{2+} channel blocker) during the night or the morning.

TEA (30 mM) caused a significant depolarization in *per1* cells recorded in the morning (from –43 ± 1.2 mV to –28 ± 0.9 mV; $P < 0.001$, $n = 8$ neurons, ANOVA and post hoc test), and significantly increased their R_{input} (1.5 ± 0.03 to 2.9 ± 0.2; $P < 0.001$, ANOVA and post hoc test) (fig. S8). Nimodipine (2 μM) depolarized *per1* cells recorded in the morning so that their cellular behaviors and RMP were similar to those *per1* cells tested in the afternoon (fig. S8). Nimodipine also caused cells whose RMP was near –33 mV to depolarize to –25 mV (fig. S8). Antagonizing L-type Ca^{2+} channels in SCN neurons inhibits Ca^{2+}-dependent K^+ channels (K_{ca}) (*15*), and in many neuronal systems inhibition of K_{ca} channels causes depolarization (*17*). So, we tested whether the large- (BK_{Ca}) and/or the small-conductance (SK_{Ca}) K_{ca} are involved in setting the RMP of *per1* neurons. Iberiotoxin (IbTX; BK_{Ca}-selective receptor antagonist) (100 nM) causes small depolarization (2 to 3 mV) in early- and late-morning *per1* cells. However, concomitant application of IbTX and apamin (SK_{Ca} selective receptor antagonist) (100 to 200 nM) during early and late morning caused significant and irreversible depolarization (13 to 15 mV) in *per1* cells, and significantly increased their R_{input} (1.6 ± 0.03 to 3 ± 0.2; $P < 0.001$) to values that were indistinguishable from those of *per1* cells measured in the afternoon (Figs. 2 and 4). During the apamin- and IbTX-induced depolarization, morning *per1* cells displayed behaviors and membrane properties that were typical of afternoon *per1* cells (figs. S9 and S10). Thus, spontaneous depolarization and associated change in R_{input} observed in *per1* neurons between dawn and dusk result from a clock-controlled reduction in BK_{Ca} and SK_{Ca} conductances. IbTX and apamin had little effect on the RMP of non-*per1* cells

during the day (fig. S11). Although TEA (n = 6 neurons) dose-dependently depolarized cells in the early-night state and increased their R_{input} to values similar to those of cells measured in the morning (Fig. 2 and figs. S8 and S12), these night effects were not seen with nimodipine, IbTX, or apamin (n = 7 neurons) (fig. S12). This suggests that BK_{Ca}, SK_{Ca}, and L-type Ca^{2+} channels minimally influence the RMP of *per1* neurons during the night.

Blocking of AP-dependent presynaptic potentials with TTX (200 nM to 1 μM; n = 8 neurons) or inhibition of postsynaptic receptors for glutamate and γ-aminobutyric acid, alone or in combination, had no effect on the RMP of *per1* cells at any time (fig. S13). This suggests that the observed changes in RMP of *per1* cells were cell autonomous and do not rely on the network properties of the SCN (*18*).

Both our experimental and modeling results establish that like invertebrate circadian clock neurons (*19*–*21*), *per1*-containing SCN cells exhibit clock-controlled, high-amplitude circadian oscillations in key electrophysiological properties. A loss of BK_{Ca} and SK_{Ca} channel conductances underpin the depolarization of RMP seen in *per1* neurons during the afternoon, whereas multiple K^+ channels contribute to hyperpolarization of these cells during the night. In contrast, SCN neurons lacking detectable EGFP expression showed much smaller day-night differences in electrophysiological parameters but do exhibit the characteristic circadian differences in AP frequency (*4*–*6*). The level of *per1*-driven EGFP peaks about two hours before the day-night transition (*4*), with its morning and dusk phases showing strong association with AP generation. However, in the middle of the afternoon, neurons containing *per1* are in an excited state but do not fire APs. This temporal dissociation between clock gene expression and AP generation, at this time of day, demonstrates that the relationships between *per1* expression and neuronal membrane properties are much more complex than first supposed (*22*–*24*). Our study also indicates that the neurophysiology of *per1* neurons may not obey conventional electrophysiological principles.

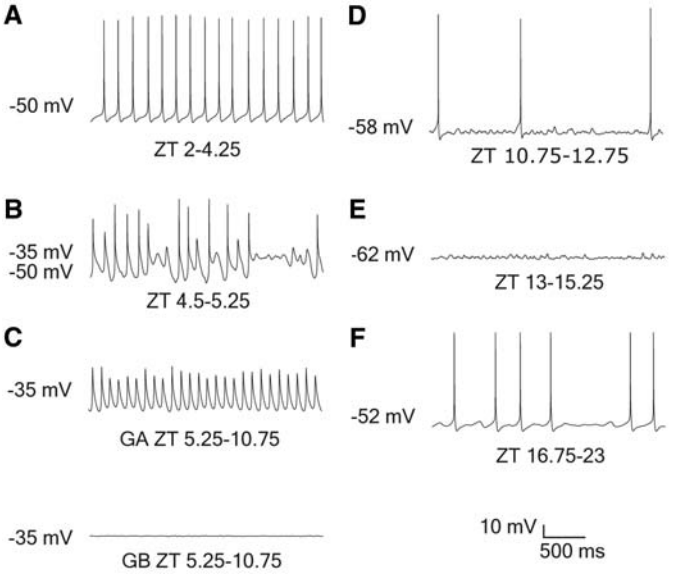

Fig. 3. Mathematical simulations predict the electrophysiological behavior of SCN clock neurons observed throughout a day-night cycle. These simulations use a revised version of the Sim-Forger model (*7*) specific for *per1* neurons and incorporate randomly generated postsynaptic potentials (fig. S2). (**A** to **F**) Panels are similar to experimental data in Fig. 1, B to G, and show that known rhythms in ionic currents (fig. S3) can explain the experimentally observed behaviors.

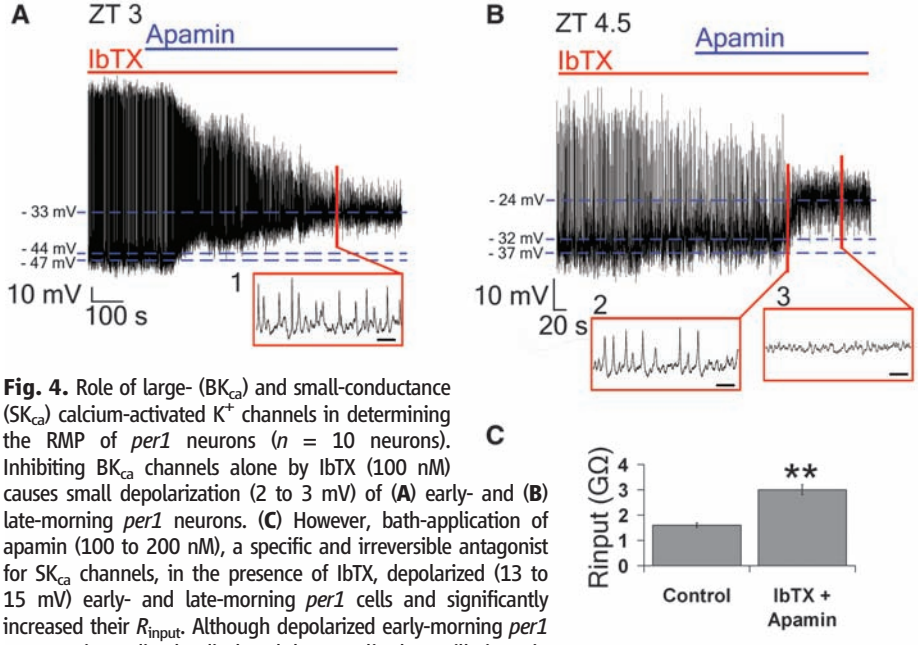

Fig. 4. Role of large- (BK_{Ca}) and small-conductance (SK_{Ca}) calcium-activated K^+ channels in determining the RMP of *per1* neurons (n = 10 neurons). Inhibiting BK_{Ca} channels alone by IbTX (100 nM) causes small depolarization (2 to 3 mV) of (**A**) early- and (**B**) late-morning *per1* neurons. (**C**) However, bath-application of apamin (100 to 200 nM), a specific and irreversible antagonist for SK_{Ca} channels, in the presence of IbTX, depolarized (13 to 15 mV) early- and late-morning *per1* cells and significantly increased their R_{input}. Although depolarized early-morning *per1* neurons immediately displayed low-amplitude oscillations in MP [(A), inset 1], late morning *per1* cells first show low-amplitude oscillations in MP during depolarization [(B), inset 2] and then became silent [(B), inset 3]. These behaviors were typical of afternoon *per1* cells (Fig. 1 and figs. S1 and S8). **P < 0.001. Numerical data represent ±SEM.

References and Notes

1. C. H. Ko, J. S. Takahashi, *Hum. Mol. Genet.* **15**, R271 (2006).
2. H. Tei *et al.*, *Nature* **389**, 512 (1997).
3. A. T. L. Hughes *et al.*, *J. Neurochem.* **106**, 1646 (2008).
4. M. U. Gillette *et al.*, *Ciba Found. Symp.* **183**, 134 (1995).
5. M. Mrugala, P. Zlomanczuk, A. Jagota, W. J. Schwartz, *Am. J. Physiol. Regul. Integr. Comp. Physiol.* **278**, R987 (2000).
6. D. J. Cutler *et al.*, *Eur. J. Neurosci.* **17**, 197 (2003).
7. C. K. Sim, D. B. Forger, *J. Biol. Rhythms* **22**, 445 (2007).
8. S. Yamaguchi *et al.*, *Science* **302**, 1408 (2003).
9. C. M. Pennartz, M. T. de Jeu, N. P. Bos, J. Schaap, A. M. Geurtsen, *Nature* **416**, 286 (2002).
10. G. R. Pitts, H. Ohta, D. G. McMahon, *Brain Res.* **1071**, 54 (2006).
11. M. Ikeda *et al.*, *Neuron* **38**, 253 (2003).
12. J. Rinzel, G. B. Ermentrout, in *Methods in Neuronal Modeling*, C. Koch, I. Segev, Eds. (MIT Press, Cambridge, MA, ed. 2, 1998), pp. 251–292.
13. D. Paydarfar, D. B. Forger, J. R. Clay, *J. Neurophysiol.* **96**, 3338 (2006).
14. E. M. Izhikevich, *Dynamical Systems in Neuroscience* (MIT Press, Cambridge, MA, 2007).
15. A. C. Jackson, G. L. Yao, B. P. Bean, *J. Neurosci.* **24**, 7985 (2004).
16. R. P. Irwin, C. N. Allen, *J. Neurosci.* **27**, 11748 (2007).
17. X. Liu, A. E. Herbison, *Endocrinology* **149**, 3598 (2008).
18. T. M. Brown, H. D. Piggins, *Prog. Neurobiol.* **82**, 229 (2007).
19. G. Cao, M. N. Nitabach, *J. Neurosci.* **28**, 6493 (2008).
20. V. Sheeba, H. Gu, V. K. Sharma, D. K. O'Dowd, T. C. Holmes, *J. Neurophysiol.* **99**, 976 (2008).
21. S. Michel, M. E. Geusz, J. J. Zaritsky, G. D. Block, *Science* **259**, 239 (1993).
22. S. J. Kuhlman, R. Silver, S. J. Le, A. Bult-Ito, D. G. McMahon, *J. Neurosci.* **23**, 1441 (2003).
23. M. J. Vansteensel *et al.*, *Curr. Biol.* **13**, 1538 (2003).
24. M. H. Hastings, E. D. Herzog, *J. Biol. Rhythms* **19**, 400 (2004).

25. We thank D. McMahon, Vanderbilt University, for providing us with the *per1*::2dGFP mice and R. Lucas and R. Baines, University of Manchester, C. Diniz Behn, University of Michigan, and D. Paydarfar, University of Massachusetts Medical School, for their critical reading of the manuscript. This work was funded by a project grant from the Biotechnology and Biological Sciences Research Council awarded to H.D.P. (BB/E00511X). M.D.C.B. is a Research Associate. C.O.D. is a NSF Graduate Research Fellow. D.B.F. is an Air Force Office of Scientific Research Young Investigator (FA 9550-08-01-0076).

Supporting Online Material

www.sciencemag.org/cgi/content/full/326/5950/281/DC1
Materials and Methods
Figs. S1 to S18
References

11 December 2008; accepted 24 August 2009
10.1126/science.1169657